PI(3,5)P_2 asymmetry during mitosis is essential for asymmetric vacuolar inheritance

Mariam Huda[1], Mukadder Koyuncu[1], Cansu Dilege[1], Ayşe Koca Çaydaşı[1]*

[1]Department of Molecular Biology and Genetics, Koç University, Istanbul, Turkey

*Correspondence to: aykoca@ku.edu.tr

Abstract

Phosphatidylinositol 3,5-bisphosphate (PI(3,5)P_2) is a low-abundance signaling lipid that plays crucial roles in various cellular processes, including endolysosomal system structure/function, stress response, and cell cycle regulation. PI(3,5)P_2 synthesis increases in response to environmental stimuli, yet how it changes in cycling cells under basal conditions remained elusive. Here, using in vivo biosensors and live cell imaging, we analyzed spatiotemporal changes in PI(3,5)P_2 levels during the cell cycle of the budding yeast *S. cerevisiae*. We established that PI(3,5)P_2 accumulates on the vacuole in the daughter cell while it disappears from the vacuole in the mother cell during mitosis. Employing a ratiometric in vivo pH sensor, we showed that the daughter vacuole is acidified while the mother vacuole gets alkalinized concomitant with the changes in PI(3,5)P_2 distribution during mitosis. Our results further suggest that the asymmetry of PI(3,5)P_2 and the PI(3,5)P_2 effector Atg18 determine the asymmetry of vacuolar pH, providing insights into how the mother cell ages while the daughter cell is rejuvenated.

Keywords

Asymmetric cell division/Aging/Atg18/Phosphatidylinositol 3,5-bisphosphate/Vacuole

Introduction

Phosphorylated phosphatidylinositol lipids (PIPs), conserved from yeast to humans, are signaling lipids that serve as master regulators of multiple cellular processes. Among the seven PIPs, Phosphatidylinositol-3,5-bisphosphate (PI(3,5)P_2) constitutes one of the least abundant and least understood PIPs. Being a PIP of the endolysosomal system, PI(3,5)P_2 plays various critical roles in diverse aspects of cell biology such as membrane trafficking, stress response, vacuole/lysosome structure/function, nutrient sensing and cell cycle regulation [1, 2, 3, 4, 5, 6, 7].

PI(3,5)P_2 is synthesized through phosphorylation of the phosphatidylinositol 3-phosphate (PI3P) by the PI3P-5kinase, PIKfyve in humans and Fab1 in yeast [8, 9]. In human cells PIKfyve localizes at endolysosomal membranes (early, late, recycling endosomes and lysosomes),

predominantly on recycling endosomes [10]. In yeast, Fab1 predominantly decorates the membrane of the vacuole (yeast lysosomes) and localizes to some extend on signaling endosomes [11]. On these membranes, PIKfyve/Fab1 resides within a protein complex composed of conserved proteins namely Vac14 (ArPIKfyve in humans) and Fig4 (Sac3 in humans) required for PIKfyve/Fab1 function [12, 13, 14, 15]. In yeast, additionally, a vacuolar membrane protein named Vac7 is part of the Fab1-complex and has an essential role in PI(3,5)P_2 synthesis [13, 16].

Under basal conditions, PI(3,5)P_2 levels are scarce; however, PI(3,5)P_2 abundance increases suddenly in response to environmental stimuli such as insulin treatment in mammalian cells and hyperosmotic shock in budding yeast [7, 9, 13, 17, 18, 19, 20]. This is best observed in budding yeast, in which PI(3,5)P_2 levels rise rapidly and transiently up to 20-fold upon hyperosmotic shock [13, 21]. The abrupt response of PI(3,5)P_2 synthesis to hyperosmotic shock made the budding yeast a great model to understand PI(3,5)P_2 regulation and function under hypertonic conditions. A growing body of evidence, however, suggests that PI(3,5)P_2 also functions in cycling cells under basal conditions [3, 4, 5, 22]. Nevertheless, low levels of PI(3,5)P_2 and lack of a well-established biosensor for in vivo detection of PI(3,5)P_2 have been obstacles to the study of PI(3,5)P_2 under isotonic conditions. In 2013, a tandem dimer of the soluble N-terminus of PI(3,5)P_2 binding protein TRPML1 was proposed as a specific in vivo probe for PI(3,5)P_2, which was later shown to bind other cellular structures disputing its use as a reliable PI(3,5)P_2 reporter [23, 24, 25]. In yeast, vacuolar localization of the PI(3,5)P_2 binding protein Atg18, which is similar to WIPI proteins in mammals, was shown to correlate well with Fab1 activity [26, 27, 28] and has been a good candidate for a PI(3,5)P_2 sensor. Yet, Atg18 also binds to PI3P (with a lesser affinity than PI(3,5)P_2) [29], and the Atg18 mutant that only binds PI(3,5)P_2 but not to PI3P (Atg18-Sloop) has also reduced binding to PI(3,5)P_2 [28], challenging its use as an in vivo sensor. Recently, a new probe, SnxA from *Dictyostelium discoideum* was identified as an extremely selective PI(3,5)P_2-binding protein [30]. Its use as a PI(3,5)P_2 reporter was characterized in mammalian cells and in *D. discoideum* [30], which provided now the means to study PI(3,5)P_2 under basal conditions.

Here, we analyzed spatiotemporal changes in PI(3,5)P_2 in budding yeast cells during an unperturbed mitosis. For this, first, we generated a yeast codon-optimized SnxA and confirmed its usage as an in vivo marker for PI(3,5)P_2 in *S. cerevisiae*. Through live cell imaging of cells during the cell cycle, we established that PI(3,5)P_2 is asymmetrically present on yeast vacuoles

during mitosis. After completion of the vacuole segregation from the mother to the daughter cell compartments, PI(3,5)P_2 accumulated on the membrane of the vacuole that resided in the daughter cell, while it disappeared from the vacuole that stayed in the mother cell. Asymmetry of PI(3,5)P_2 was established shortly before anaphase onset, maintained during anaphase, and diminished with mitotic exit. Next, as an independent approach to SnxA localization, we established the use of Atg18, a PI(3,5)P_2 binding protein yeast, as a PI(3,5)P_2 probe. Atg18-mNeongreen localized preferentially to the daughter vacuole periphery in the same way as SnxA-GFP, confirming PI(3,5)P_2 asymmetry during mitosis. Considering the role of PI(3,5)P_2 in vacuolar acidity, we employed a ratiometric in vivo pH sensor to observe changes in vacuolar pH during mitosis. Our data showed that the daughter vacuole is acidified while the mother vacuole gets alkalinized concomitant with the changes in PI(3,5)P_2 distribution during mitosis. Analyzing mutants with symmetric PI(3,5)P_2 distribution, we further showed that the asymmetry of PI(3,5)P_2 and the PI(3,5)P_2 effector Atg18 determine the asymmetry of vacuolar pH. Intriguingly, cells with symmetric PI(3,5)P_2 distribution had a longer chronological life span, suggesting that the PI(3,5)P_2 asymmetry ensures that daughter cells receive more acidic vacuoles, whereas the vacuoles of the mother cells get alkalinized in every cell division. Our data thus provide insights into how yeast cells safeguard mother cell aging and daughter cell rejuvenation in each cell division.

Results

Yeast codon optimized SnxA can be used as an in vivo sensor for PI(3,5)P_2 in budding yeast

In order to monitor PI(3,5)P_2 in budding yeast, we sought to make use of the recently identified genetically coded PI(3,5)P_2 sensor SnxA, which was tested in mammalian cells and in amoebae [30]. To address whether SnxA would work as an in vivo PI(3,5)P_2 sensor in budding yeast, first, we constructed yeast codon-optimized SnxA C-terminally fused with GFP and expressed under TEF1 promoter (Figure S1A). Expression of SnxA-GFP integrated into the yeast genome did not alter the vacuole size or cell growth, indicating that SnxA expression does not interfere with PI(3,5)P_2 function (Figure S1B-C). SnxA-GFP colocalized with the vacuolar membrane marker Vph1-3xmCherry in wildtype yeast cells, assessed by Pearson Correlation Coefficient (PCC) obtained through EzColocalization plugin in ImageJ (Figure 1A) [31]. Colocalization was lost in the absence of the PI 5-kinase *FAB1*, as well as the absence of *VAC7* or *VAC14* which are essential for PI(3,5)P_2 synthesis (Figure 1A). Thus, we conclude that SnxA vacuole

membrane localization is PI(3,5)P_2 dependent in budding yeast. In line with this notion, SnxA co-localization with Vph1 increased in cells expressing a hyperactive Fab1 allele (*fab1-ha, fab1-14)* [16], which leads to overproduction of PI(3,5)P_2 (Figure 1B). Likewise, *fab-ha* expression fully rescued the loss of SnxA vacuole localization in *vac14*Δ cells and markedly increased SnxA colocalization with Vph1 in *vac7*Δ cells (Figure 1B), which is consistent with *fab-ha* rescue of PI(3,5)P_2 levels in these cells [16, 32].

It is well established by biochemical methods that the amount of PI(3,5)P_2 increases drastically but transiently in response to hyperosmotic shock in budding yeast [13, 21] – such that within 5 minutes after hyperosmotic shock (0.9M NaCl treatment) PI(3,5)P_2 levels increase ~20 fold, elevated PI(3,5)P_2 persists for ~10 min, after which it starts decreasing, and restores near basal levels ~30 minutes after initial exposure to hyperosmotic shock [13]. Hence, to capture the condition with high PI(3,5)P_2 levels, we measured SnxA-GFP vacuole periphery localization ~10 min after 0.9M NaCl treatment. SnxA colocalization with Vph1 increased dramatically upon hyperosmotic shock of logarithmically growing wildtype cells (Figure 1C). Salt treatment also caused an increase in SnxA-GFP vacuole localization in *vac14*Δ cells but not in *vac7*Δ and *fab1*Δ (Figure1C), which is in line with previous data that hyperosmotic shock triggers PI(3,5)P_2 production in *vac14*Δ cells, albeit at a low level, but not in *vac7*Δ and *fab1*Δ cells [13]. We further quantified SnxA vacuole localization upon hyperosmotic shock through time-lapse microscopy. Colocalization of SnxA-GFP with Vph1-3xmCherry prominently increased within the first 2 min following hyperosmotic shock (Figure 1D). High levels of SnxA colocalization with Vph1 were maintained for ~7 min, after which it started decreasing (Figure1D-E). Colocalization was diminished ~30 min after the hyperosmotic shock (Figure1D-E), in a similar manner measured by biochemical methods [13]. Taken together, these data establishes that SnxA can be used as an in vivo sensor for PI(3,5)P_2 in budding yeast, similar to its usage in amoeba and mammalian cells [30].

More PI(3,5)P_2 is present on the daughter vacuole during yeast mitosis

While assessing SnxA-GFP colocalization with Vph1-3xmCherry, we noticed that in cells with segregated vacuoles, SnxA-GFP localization on the vacuole periphery was asymmetric, with a strong preference to localize on the vacuole that resides in the daughter cell compartment (daughter vacuole) (Figure 1A and 2A). On the vacuole of the mother cells (mother vacuole), however, SnxA-GFP was barely detectable (Figure 1A and 2A).

Next, we asked when SnxA asymmetry was established. To this end, we performed time-lapse microscopy of Vph1-3xmCherry SnxA-GFP containing cells. SnxA-GFP signal was low or undetectable on the vacuole while the vacuole was being segregated to the daughter cell (Figure 2B-C). Within 3 minutes after completion of vacuole segregation (t=0), SnxA-GFP accumulated on the daughter vacuole (Figure 2D, Supplementary movie 1, Figure S2 – individual cells). SnxA-GFP signal persisted for ~21 min at the daughter vacuole, after which the signal was greatly reduced (Figure 2E). Quantification of SnxA vacuole periphery localization dynamics revealed that SnxA asymmetry increased for ~15-18 min after vacuole segregation (Figure 2C). During this time SnxA localization on the daughter vacuole increased, whereas it was completely diminished from the mother vacuole (Figures 2B-C). After this period, SnxA localization to the daughter vacuole started to decrease, concomitant with a slight increase of SnxA localization on the mother vacuole, causing a decrease in the SnxA asymmetry (Figures 2B-C, Supplementary movie 1). Finally, SnxA localized weakly but equally on both vacuoles, reaching a nearly symmetric state (Figures 2B-C). Using GFP-Tub1 as a mitotic marker, we next addressed when during the cell cycle SnxA-mCherry accumulates on the daughter vacuole. Time-lapse microscopy of GFP-Tub1 SnxA-mCherry containing cells showed that SnxA accumulation on the daughter vacuole started 3±2 min (mean±SD) before anaphase onset, whereas disappearance of the SnxA-mCherry signal on the daughter vacuole happened near mitotic exit (±5 min) (Figure 2F, Supplementary movie 2).

Considering that SnxA on the vacuolar membrane reflects the PI(3,5)P_2 levels, we conclude that PI(3,5)P_2 is indeed synthesized in cycling cells under basal conditions. It peaks on the daughter vacuole during mitosis, whereas it disappears from the mother vacuole, creating an asymmetry. PI(3,5)P_2 asymmetry is, however, interrupted after mitotic exit.

Atg18 localization at the vacuole periphery correlates with PI(3,5)P_2 levels and mimics SnxA localization

As an alternative way to measure PI(3,5)P_2 levels on vacuolar membranes in living cells, we next analyzed the localization of Atg18, a known protein that binds PI(3,5)P_2 with higher affinity, and PI3P with a lower affinity [26, 27, 28, 33]. PI(3,5)P_2 binding pool of Atg18 associates with the vacuolar membrane [28]. In concordance with this, wildtype Atg18-mNeongreen colocalized with Vph1-3xmCherry in logarithmically growing cells upon hyperosmotic shock (Figure S3A). Atg18-SlooP mutant, which binds PI(3,5)P_2 but not PI3P [28], also colocalized with Vph1; whereas the Atg18-FGGG mutant that does not bind PI(3,5)P_2 and PI3P [28] failed

to localize on the vacuolar membrane (Figure S3A). Atg18-mNeongreen also colocalized with Vph1 under basal conditions (Figure S3B). Hyperosmotic shock or expression of *fab1-ha* increased colocalization of Atg18-mNeongreen with Vph1 (Figure S3B) whereas, deletion of *VAC7* or *VAC14* diminished Atg18 vacuole periphery localization (Figure S3B). Similar to the results obtained using SnxA, *fab1-ha* rescued vacuole localization of Atg18 in both *vac7*Δ and *vac14*Δ cells, whereas salt treatment only rescued vacuole localization in *vac14*Δ (Figure 3B). Accordingly, we conclude that Atg18 localization at the vacuole periphery is indicative of PI(3,5)P_2 levels. Furthermore, time-lapse analysis of Atg18-mNeongreen colocalization with Vph1-3xmCherry yielded similar results to that of SnxA (Figure 3). Atg18 explicitly localized to the vacuole that migrated to the daughter cell, but not to the vacuole that stayed in the mother cell in mitosis (Figure 3A-B, Figure S4) with similar timing as SnxA (Figure 3C-E). Thus, using two independent PI(3,5)P_2 in vivo markers, Atg18 and SnxA, these results altogether establish that PI(3,5)P_2 is specifically present on the daughter vacuole of the yeast during mitosis, whereas it diminishes from the mother vacuole.

Levels of PI3P and Fab1-complex components are symmetrically distributed on the mother and daughter vacuole

We reasoned that the asymmetry of PI(3,5)P_2 may stem from differential levels of its precursor, PI3P, on mother and daughter vacuoles. To understand whether this is the case, we monitored PI3P in living cells using FYVE domain of mammalian Hrs [34, 35]. Unlike PI(3,5)P_2, GFP-2xFYVE localized equally on mother and daughter vacuoles (Figure 4A). Thus, PI(3,5)P_2 asymmetry is unlikely to be due to PI3P levels. Alternatively, PI(3,5)P_2 asymmetry may stem from asymmetric distribution of Fab1, Vac7, and Vac14 proteins, which altogether constitute the Fab1-complex. Nevertheless, unlike Atg18, neither of these proteins were asymmetrically distributed on mother and daughter vacuoles (Figure 4B), suggesting that it is the activity of the Fab1 rather than the levels of Fab1-complex proteins on vacuoles that determine the asymmetry of PI(3,5)P_2. Supporting this hypothesis, expression of the hyperactive form of Fab1 (*fab1-ha*) resulted in not only an increment of PI(3,5)P_2 levels but also promoted equal levels of PI(3,5)P_2 on both vacuoles, breaking the PI(3,5)P_2 asymmetry (Figure 4C). Similarly, elevation of Fab1 activity by deletion of *ATG18* [27], also disrupted PI(3,5)P_2 asymmetry (Figure 4C).

Asymmetry of vacuolar pH is established concomitant with PI(3,5)P_2 asymmetry

Facilitating the assembly and activity of Vph1 containing vacuolar H^+-ATPase (V-ATPase), PI(3,5)P_2 functions in vacuole acidification, [36, 37]. Of importance, vacuolar pH also exhibits an asymmetric behavior between mother and daughter cells, such that the daughter vacuole is more acidic than the mother vacuole already before cytokinesis [38, 39]. We thus asked whether daughter vacuole acidification coincides with PI(3,5)P_2 accumulation on the daughter vacuole. To this end we performed time-lapse microscopy using the vSEP-mCherry ratiometric pH sensor [40]. In this ratiometric pH sensor, the vacuole-targeted acid-sensitive fluorophore vSEP is fused with pH-insensitive fluorophore mCherry. Hence, the vSEP/mCherry ratio correlates with the pH. We quantified the vSEP/mCherry ratio in daughter and mother vacuoles separately, with respect to the timing of vacuole segregation (Figure 5A, Supplementary movie 3). Using our previous data that established dynamic changes of PI(3,5)P_2 as a reference (Figure 2C), we compared the changes in vSEP/mCherry ratio with the changes in PI(3,5)P_2 asymmetry. Our results showed that, shortly after the establishment of PI(3,5)P_2 asymmetry, the daughter vacuole started to acidify rapidly, while the mother vacuole started to get alkalinized (Figure 5A). This suggests that acidification of the daughter vacuole follows elevation of PI(3,5)P_2 levels on the daughter vacuole, whereas alkalinization of the mother vacuole follows the diminishment of PI(3,5)P_2 on the mother vacuole. Supporting this view, concomitant with the reappearance of PI(3,5)P_2 on the mother vacuole (Figure 2C, 18-24 min), the mother vacuole started to regain its acidity (Figure 5A, 18-24 min). Upon establishment of symmetric PI(3,5)P_2, both mother and daughter vacuole pH exhibited similar behavior over time. However, the daughter vacuole remained more acidic than the mother vacuole. Our data thus shows that the vacuolar pH is established soon after vacuole segregation and further indicates that changes in PI(3,5)P_2 asymmetry correlate with changes in the vacuolar pH.

PI(3,5)P_2 and its asymmetry are crucial for the asymmetry of vacuolar pH and longevity

In order to understand whether PI(3,5)P_2 and its asymmetry are required for vacuole acidity and asymmetry of the vacuolar pH, we analyzed vacuolar pH in the absence of PI(3,5)P_2 (using *vac7*Δ cells) and under conditions that yield symmetric PI(3,5)P_2 distribution. To obtain cells with symmetric PI(3,5)P_2 distribution, we first made use of *fab1-ha* expressing cells. We measured vSEP/mCherry ratios in cells with segregated vacuoles. Mother vacuole of wildtype cells had higher vSEP/mCherry ratios than the daughter vacuoles (Figure 5B), consistent with previous reports [38, 39] and our time-lapse data (Figure 5A). Deletion of *VAC7* caused a remarkable alkalinization of both vacuoles supporting the function of PI(3,5)P_2 in vacuole

acidity (Figure 5B). Intriguingly, *VAC7* deletion also resulted in relatively more alkaline daughter vacuoles than the mother vacuoles, a situation opposing wildtype cells. *fab1-ha* expression, however, caused more acidic vacuoles and symmetric distribution of pH among the daughter and mother vacuoles in wildtype cells (Figure 5B). Furthermore, *vac7*Δ cells expressing *fab1-ha* had symmetric vacuolar pH, while the overall vacuolar acidity resembled that of the daughter vacuole of the wildtype cells (Figure 5B). Likewise, in line with the contribution of vacuole acidity to yeast lifespan [39], *fab1-ha* expression prolonged the chronological life span of wildtype cells (Figure 5C). Importantly *fab1-ha* expressing *vac7*Δ cells also had a prolonged lifespan compared to wildtype cells (Figure 5C), suggesting that it's the presence of PI(3,5)P_2 on both the mother and daughter vacuoles rather than elevated levels of PI(3,5)P_2 that promoted longer lifespan. These data altogether support that PI(3,5)P_2 is required for vacuole acidification and further suggest that asymmetry of PI(3,5)P_2 is crucial for asymmetry of vacuolar pH, and hence, is linked to yeast aging and longevity.

PI(3,5)P_2-mediated vacuole acidification largely depends on Atg18

Next, we analyzed the vacuolar pH in *atg18*Δ cells in which PI(3,5)P_2 appears symmetric on the daughter and mother vacuoles (Figure 4C). However, unexpectedly, we observed that *atg18*Δ cells had overall more alkalinized vacuoles, and similar to *vac7*Δ cells, the asymmetry of vacuolar pH was reversed such that the mother vacuoles were more acidic than the daughter vacuoles (Figure 6A). Analysis of vacuolar pH in *atg18*Δ cells through time-lapse microscopy confirmed the reversed asymmetry of the vacuolar pH (Figure 6B, Supplementary movie 4). Furthermore, vacuolar pH dynamics in the mother appeared more stable during mitosis in *atg18*Δ cells compared to the wildtype cells (Figure 6B), which is in support of a previous report [40]. Thus, Atg18 is critical for vacuole acidity as well as asymmetry and dynamic aspects of vacuolar pH.

Vacuole acidity of *atg18*Δ cells was fully rescued by the Atg18-Sloop mutant that localizes to the vacuole membrane through binding to PI(3,5)P_2 (Figure 6C). Introduction of the Atg18-FGGG mutant that cannot bind membranes, however, only partially rescued vacuolar pH (Figure 6C), suggesting that Atg18 vacuole periphery localization is necessary for vacuole acidity. Considering that Atg18 vacuole periphery localization requires its binding to PI(3,5)P_2, we propose that Atg18 may have a role downstream of PI(3,5)P_2 in vacuole acidification. We reasoned that if this were the case, artificial recruitment of Atg18 on the membrane of both vacuoles would lead to mother vacuole acidification and symmetric pH. In order to target

Atg18 on both mother and daughter vacuoles, we tagged endogenous Vph1 and Atg18 at their C-terminus with GFP-binding protein (GBP) and GFP, respectively [41]. This strategy successfully provided symmetric localization of Atg18 on the periphery of both vacuoles (Figure S5). Constitutive presence of Atg18 on both vacuoles did not alter PI(3,5)P_2 asymmetry (Figure 6D), yet caused more acidic and symmetric vacuolar pH (Figure 6E, WT vs Atg18-GFP/GBP). This data supports the role of vacuole membrane localized Atg18 in vacuole acidification. However, PI(3,5)P_2 presence was essential for this role as constitutive targeting of Atg18 to the vacuolar membranes in *vac7*Δ cells had only a minor effect on vacuole acidity (Figure 6E, *vac7*Δ vs *vac7*Δ Atg18-GFP/GBP).

Collectively, these data suggest that the absence of PI(3,5)P_2 from the mother vacuole and its accumulation on the daughter vacuole during mitosis is part of a mechanism that causes alkalinization of the mother vacuole and acidification of the daughter vacuole. Vacuole acidification also requires Atg18, which is recruited to the vacuolar membrane via PI(3,5)P_2.

Discussion

In this study, we reveal that the vacuolar signaling lipid PI(3,5)P_2 is asymmetrically distributed on yeast vacuoles during mid-to-late mitosis and this asymmetry is critical for the asymmetry of vacuolar pH, and thus for differential longevity of mother and daughter cells (Figure 7).

Spatiotemporal changes in PI(3,5)P_2 distribution during mitosis

PI(3,5)P_2 is a conserved signaling lipid involved in various cellular functions, however understanding of its dynamics has been limited to changes in its global levels in response to environmental changes such as upon osmotic shock in budding yeast. One of the barriers in the field has been the lack of a well-established biosensor to detect PI(3,5)P_2 in vivo. Here, we employed chromosomally integrated yeast codon-optimized SnxA [30] and the yeast endogenous protein Atg18 as in vivo PI(3,5)P_2 probes and established their usage as PI(3,5)P_2 sensors suitable for live cell imaging in budding yeast. We show that both SnxA-GFP and Atg18-mNeongreen specifically localize to the vacuolar membrane in a PI(3,5)P_2-dependent manner, and their colocalization with the vacuolar marker Vph1 has been rigorously analyzed in a quantitative manner under various conditions, including hyperosmotic shock and genetic perturbations. These probes have allowed real-time monitoring of PI(3,5)P_2 within the cell during the cell cycle. Our results showed that PI(3,5)P_2 accumulates on the daughter vacuole, while being depleted from the mother vacuole during mitosis, creating a cellular asymmetry.

$PI(3,5)P_2$ asymmetry was established soon after vacuole segregation was completed and shortly before anaphase onset. Asymmetry was maintained throughout anaphase and diminished after mitotic exit, indicating compartment-specific and cell cycle-dependent $PI(3,5)P_2$ regulation of synthesis.

Mechanism of $PI(3,5)P_2$ asymmetry

Mechanisms underlying the establishment of $PI(3,5)P_2$ asymmetry appear to be independent of the precursor PI3P and the distribution of Fab1-complex components Fab1, Vac7, and Vac14. Our data that a hyperactive *FAB1* allele (*fab1-ha*) breaks this asymmetry indicates that the activity of Fab1, rather than its abundance, plays a critical role in generating $PI(3,5)P_2$ asymmetry. This finding points to a regulatory mechanism that increases Fab1 activity specifically on the daughter vacuole or inhibits Fab1 activity specifically on the mother vacuole, resulting in asymmetric production of $PI(3,5)P_2$. An alternative to this model could be asymmetric segregation of the $PI(3,5)P_2$-containing vacuolar membranes to the daughter cell, leaving the $PI(3,5)P_2$ deficient membranes behind. Given the role of $PI(3,5)P_2$ in vacuole segregation [42], we cannot completely rule out this alternative scenario. Nevertheless, considering the *fab1-ha* data, we favor that asymmetry of $PI(3,5)P_2$ likely stems from compartment-specific regulation of one or more Fab1-complex proteins to yield differential Fab1 activity on the mother and daughter vacuoles. Timing of $PI(3,5)P_2$ accumulation and diminishment with respect to the cell cycle suggests that one or more components of the Fab1-complex may also be subjected to cell cycle-dependent regulation. Further work will shed light on the molecular mechanisms behind $PI(3,5)P_2$ asymmetry.

$PI(3,5)P_2$ asymmetry and vacuolar pH

$PI(3,5)P_2$ interacts with Vph1 and is required for the assembly and activity of Vph1 containing vacuolar H^+-ATPase (V-ATPase), which is responsible for pumping protons into the vacuole, thereby acidifying its lumen [36, 37]. Vacuolar pH also exhibits an asymmetric distribution. Daughter cells have more acidic pH than the mother cells [38]. This asymmetry in vacuolar pH was shown to be present before the mother and daughter cells are physically separated [39], however the exact timing of when vacuolar pH asymmetry is established has been elusive. Here, we monitored vacuolar pH during mitosis using a ratiometric in vivo pH sensor [40]. Establishment of vacuolar pH asymmetry coincided with that of $PI(3,5)P_2$ asymmetry: As $PI(3,5)P_2$ increased on the daughter vacuole, daughter vacuole got acidified. Likewise, the mother vacuole got alkalinized as $PI(3,5)P_2$ disappeared from the mother vacuole. This

correlation between PI(3,5)P_2 and vacuolar acidity is in support of the function of PI(3,5)P_2 in the assembly and activation of the V-ATPase and, hence, vacuole acidification. Furthermore *fab1-ha* and *vac7*Δ *fab1-ha* mutants that had symmetrically distributed PI(3,5)P_2 had symmetric vacuolar pH, whereas *vac7*Δ cells lacking PI(3,5)P_2 had vacuoles with disrupted acidity, suggesting that the vacuolar pH asymmetry majorly stems from PI(3,5)P_2 asymmetry.

We furthermore unexpectedly discovered that vacuole localization of the PI(3,5)P_2 binding protein Atg18 is also essential for vacuole acidification and vacuolar pH asymmetry. Accordingly, *atg18*Δ cells had less acidic vacuoles with a disrupted asymmetry of pH, while forced localization of Atg18 to the periphery of both vacuoles resulted in symmetric and lower vacuolar pH. However, bringing Atg18 to the vacuole periphery in the absence of PI(3,5)P_2 did not promote vacuole acidification, highlighting the critical role of PI(3,5)P_2 in this process. How does Atg18 promote vacuolar acidity? Atg18 may work together with PI(3,5)P_2 to support V-ATPase assembly and activity, yet Atg18 has not been reported to bind V-ATPase subunits, making this notion unlikely. Considering the role of Atg18 in the cytoplasm to vacuole targeting, which provides selective transport of vacuolar enzymes to the vacuole [43, 44], we favor that the role of Atg18 in vacuole acidification may be related to vacuole biosynthesis and maturation. In that case, this function of Atg18 is likely not through sorting of Vph1 to the vacuole [45], as Vph1 localization to the vacuolar membrane seemed not affected by *ATG18* deletion. The role of Atg18 in vacuole acidification may as well be through its function in autophagy as autophagy was shown to be required for vacuole acidification [46]. Further work will be necessary to decipher the molecular link between Atg18 and vacuolar pH.

Of importance, a previous study that focused on the pH of the mother vacuoles showed that the vacuole alkalinizes before cell division and re-acidifies as cells divide. This oscillation of vacuolar pH was also found to be dependent on PI(3,5)P_2 and Atg18 among other proteins [40]. Our results are in parallel with these findings, and further describe how the pH of daughter vacuole changes during the cell cycle, and how pH of both vacuoles behaves with respect to the levels of PI(3,5)P_2-Atg18. Thus our work establishes a link between PI(3,5)P_2-Atg18 asymmetry and vacuolar pH asymmetry.

Implications for Cell Aging, Rejuvenation and genomic stability

Cellular asymmetries are fundamental to the asymmetric cell division. During asymmetric cell division of budding yeast, the mother and daughter cells receive distinct sets of organelles,

proteins, and RNAs, leading to differences in their cellular fates. This process is especially crucial for longevity and aging. A key factor contributing to yeast aging is the decline of vacuolar pH. Our results suggest that the PI(3,5)P_2 asymmetry in mitosis ensures daughter cells have more acidic vacuoles whereas mother cells have more alkaline vacuoles. Therefore, we propose that PI(3,5)P_2 asymmetry is one of the mechanisms that leads to the aging of the mother cell and rejuvenation of the daughter cell. Supporting our hypothesis, *fab1-ha* and *vac7*Δ *fab1-ha* mutants had an extended chronological lifespan.

We have previously shown that PI(3,5)P_2 promotes mitotic exit through inhibition of the Spindle Position Checkpoint (SPOC) kinase Kin4 [4]. Our current study, describing the preferential presence of PI(3,5)P_2 on the daughter vacuole, supports that PI(3,5)P_2 inhibition of Kin4 activity is restricted to the daughter cell only. While this mechanism ensures timely mitotic exit of cells with normally positioned spindles, production of PI(3,5)P_2 on both the mother and daughter vacuoles through the use of *fab1-ha* mutants caused SPOC deficiency, leading to genomic instability [4]. This data indicates that the presence of PI(3,5)P_2 on the mother vacuole would compromise maintenance of ploidy and genomic stability. Thus, we propose that PI(3,5)P_2 asymmetry provides daughter cell rejuvenation, which however comes with the expanse of mother cell aging in order to maintain genomic stability.

Methods

Yeast methods, strains, and plasmids

All yeast strains used in this study are isogenic with S288C and are listed in Table S1. Basic yeast methods and growth media were as described previously [47]. All yeast strains were grown at 30°C and in a glucose-containing medium. The cassette PCR-based gene editing method was used for gene deletion and C-terminal tagging of endogenous proteins [48, 49]. v-SEP-mCherry containing strains were obtained as described by [40]. GFP-Tubulin, mCherry-Tubulin, SnxA-GFP, SnxA-mCherry, and *fab1-ha* containing yeast were obtained by genome integration of corresponding plasmids. Plasmids used in this study are listed in Table S2.

SnxA containing plasmids were generated as follows: The SnxA-GFP sequence [30] was codon optimized for yeast and synthesized in the pUC18 plasmid under XbaI and SalI restriction sites (pHM001). SnxA-GFP fragment excised by XbaI and SalI was subsequently ligated under TEF1 promoter and CYC1 terminator sequences on p415TEF. The TEF1-SnxA-GFP-CYC fragment was then excised using KpnI and SacI and subcloned into pRS306 to yield pHM007.

pHM007 is linearized by ApaI digestion for integration into the *URA3* locus. To construct the SnxA-mCherry containing plasmid, mCherry excised from pAK011 using XhoI and BamHI was used to replace GFP in pHM001. SnxA-mCherry fragment was subcloned under TEF1 promoter and CYC1 terminator sequences on p415TEF using XbaI and SalI. Finally, the TEF1-SnxA-mCherry-CYC fragment was excised using KpnI and SacI and ligated into pRS306 and pRS304 to yield pHM009 and pHM011 respectively. pHM009 was digested with ApaI to integrate into *URA3* locus, whereas pHM011 was digested with Kpn2I for integration into *TRP1* locus.

For integration of Atg18 mutants into the endogenous locus: ~4,3kb Atg18-eGFP-klTRP1 fragment amplified from the chromosomal DNA of Atg18-eGFP-klTRP1 containing yeast strain was cloned into pRS315/XmaI&SacII to obtain pCD001. FGGG and Sloop variant containing plasmids (pCD002, pCD003) were obtained through site-directed mutagenesis of pCD001. Atg18-eGFP-klTRP1 fragments of these plasmids were amplified and used as cassettes to replace *atg18Δ::hphNT1* in CDY53.

Fluorescence Imaging

All microscopy experiments were conducted using a Carl Zeiss Axio Observer 7 motorized inverted epifluorescence microscope, equipped with a Colibri 7 LED light source, Axiocam 702 Monochrome camera, 63× Plan Apochromat immersion oil objective lens, Zeiss filter sets 95 (GFP/Cherry) and 44 (FITC), and an XL incubation and climate chamber.

For time-lapse experiments, cells were grown in filter-sterilized SC-complete media to the log phase and attached to glass-bottom Petri dishes (WVR 10810-054 Matsunami) as previously described [50]. Briefly, the center of the glass dish was coated with 6% Concanavalin A (*Canavalia ensiformis* Jack Bean, type IV Sigma C2010-G) for 10 minutes, then rinsed with sterile water. Next, 200 µL of a logarithmic phase culture was added to the center of the dish and incubated at 30°C for 30 minutes. Non-attached cells were removed by washing with pre-warmed media. The dish was filled with pre-warmed media, placed on the microscope stage, and allowed to sit for 1 hour before starting the experiment. The microscope chamber was preheated to 30°C, 2-3 hours before the experiment. For time-lapse experiments that monitored response to hyperosmotic shock, the glass-bottom petri dish was initially filled halfway with prewarmed media. Once the experiment commenced, 1.8M NaCl dissolved in filter-sterilized SC-Complete media was carefully added at 1:1 ratio (v:v) into the dish on the microscope.

Time-lapse experiments involving SnxA-GFP without hyperosmotic shock, 3xmCherry-Tubulin, and v-SEP-mCherry *atg18*Δ were conducted with images taken at 3-minute intervals. For Atg18-mNG Vph1-3xmCherry, images were captured at 5-minute intervals. Imaging frequency for GFP-Tubulin, Atg18-mNG Vph1-3xmCherry without hyperosmotic shock and v-SEP-mCherry WT, the interval was set at 1-minute intervals.

Still images of cells were captured without cell fixation. Briefly, 1 mL of log-phase culture grown in filter sterilized SC-complete was centrifuged at 3200 rpm for 2 minutes, and cells were resuspended in an appropriate volume of SC-Complete medium before wet mount preparation. A maximum of 3 images were acquired immediately from each slide to prevent stressing of the cells and photobleaching of the signals. For the still images involving hyperosmotic shock, cell suspensions were mixed with 1.8M NaCl containing filter sterilized SC-Complete media at a ratio of 1:1 (v:v) and imaged between 5-10 minutes after salt addition.

Imaging conditions were as follows: v-SEP-mCherry was imaged using the FITC channel at 5% and the mCherry channel at 10%. SnxA-GFP was captured using the FITC channel at 10%. Vph1-3xmCherry and 3xmCherry-Tubulin were imaged using the mCherry channel at 10%. SnxA-mCherry utilized the mCherry channel at 20%, GFP-Tubulin used the FITC channel at 20%, and Atg18-mNG was imaged using FITC at 15%. 2x2 binning was applied during acquisition. For still images, 13 z-stacks of 0,3 µm thickness were acquired per image. For time-lapse experiments, 9 z-stacks of 0,4 µm thickness were acquired per image.

Assessing timing of SnxA and Atg18 vacuole localization

The temporal localization of SnxA and Atg18 on vacuole membranes with respect to vacuole segregation and spindle elongation was judged by eye through monitoring of individual cells from the time-lapse series using Image J (NIH) software.

For the timing with respect to vacuole segregation, all cells in which segregation of the vacuole can be observed were inspected. Vacuole segregation process usually involves vesicle movement from the mother to daughter at several steps. The end of vacuole segregation was marked as the point after which vesicle movement was not observed. Timepoints at which a clear SnxA or Atg18 fluorescent signal was detected at the mother or daughter vacuole peripheries were noted. The time points of signal appearance and/or disappearance were recorded. Signal persistence was calculated as the duration between signal appearance and

disappearance. Timing of signal appearance was calculated as the time between end of vacuole segregation and signal appearance.

For the timing with respect to spindle elongation, all cells that underwent both the metaphase-to-anaphase transition and the spindle breakdown during the time-lapse duration were analyzed. The timepoints for anaphase onset and spindle breakdown were determined by observing when rapid spindle elongation and spindle breakdown first occurred. The timing of SnxA-GFP and Atg18-mNG signal appearance on the daughter vacuole was calculated with respect to the timing of anaphase onset (t=0). The timing of SnxA-GFP and Atg18-mNG signal disappearance from the daughter vacuole was calculated with respect to the timing of spindle breakdown. To be able to show both timings on the same graph, spindle breakdown timing was normalized to 20 minutes for each cell.

Assessing vacuole periphery localization via EzColocalization

To calculate Pearson Correlation Coefficient (PCC) values of Atg18/SnxA/FYVE and Vph1 signals, z-projection were performed by summing 4 z-stacks, in which the vacuole was in focus based on the Vph1 reference. Using two reporter inputs and the ROI manager for cell identification, the EzColocalization plugin ImageJ (NIH, Bethesda, Maryland, United States) was used to determine the PCC between Atg18/SnxA/FYVE and Vph1. First, the vacuole periphery was manually selected from the Vph1 channel using the oval selection tool and added to the ROI manager. In the EzColocalization window, PCC was selected, with the ROI set for cell identification.

PCC values from time-lapse experiments were obtained in the same way, this time the process was repeated per cell for multiple consequent time points. The time point of end of vacuole segregation (see the section above) was also noted based on Vph1 signal. The PCC values were then aligned according to this timing, mean PCC per timepoint were plotted.

Measurement of vacuole diameter

Vacuole diameters were measured using the measure tool on maximum projected images, using ImageJ.

Assessing Protein Asymmetry on Mother and Daughter Vacuoles:

For analysis of protein asymmetry on mother and daughter vacuoles, z-stacks were sum-projected. Daughter to mother ratios of proteins of interest (Figure 4B) were determined using the following equation: $\frac{d[(g_v-g_{bg})/(r_v-r_{bg})]}{m[(g_v-g_{bg})/(r_v-r_{bg})]}$; where *m* and *d* represent mother and daughter vacuoles respectively, *g* denotes mean fluorescence intensity of mNG/GFP (green signal), *r* means mean fluorescence intensity of mCherry (red signal), *v* indicates signal on the vacuole, and *gb* and *rb* represents the cytosolic signal (background) in the green and red channels respectively. Vacuoles were selected using oval selection tool based on Vph1-3xmCherry signals. Briefly, the same area was used to measure the mean fluorescence intensity of Vph1-3xmCherry and the protein of interest tagged with GFP/mNG. Mean fluorescence intensities were corrected for the background signal by subtracting the cytoplasmic signal from the vacuolar signal. Signal of the protein of interest was normalized by the Vph1-3xmCherry mean fluorescence intensity to obtain the relative levels of protein of interest per unit vacuole membrane (Vph1-3xmCherry serves as a reference). Normalized values of daughter and mother vacuoles were divided to obtain daughter to mother ratios of the protein per unit vacuole membrane.

Analysis of vacuolar pH:

For analysis of vacuolar pH, z-stacks were sum-projected using ImageJ. Using the oval selection tool, the central region of the vacuole was selected based on mCherry signal. Mean fluorescence intensity of this area was measured in both the v-SEP and mCherry channels. The mean fluorescence intensity of an area free from cells was also measured as the background. Mean fluorescence intensities of v-SEP and mCherry were corrected for background signal by subtracting the background signal from the vacuolar signal. vSEP/mCherry was calculated by dividing the corrected v-SEP signal by the corrected mCherry signal. vSEP/mCherry ratios from time-lapse experiments were obtained in the same way. The time point of end of vacuole segregation was also noted based on mCherry signal. vSEP/mCherry ratios were then aligned according to this time point, vSEP/mCherry ratios per timepoint were plotted.

Chronological Life Span analysis

The chronological lifespan (CLS) experiment was conducted following the method outlined by [51]. Experiment was performed in 3 biological replicates. Briefly, strains were grown to the stationary phase in autoclaved SC-Complete media at 30°C and then diluted to an OD_{600} of 0.1

in 10 mL. Cultures were further incubated at 30°C in foil-capped tubes with a media-to-air ratio of 1:5. Starting from day 6, every other day, two samples from each strain were taken (2 technical replicates), diluted to 1:10,000 in autoclaved sterile water, and 10 µL of this dilution was plated on YPD plates and incubated at 30°C. Colony-forming units (CFUs) were counted after 2 days of growth on YPD. This sampling process was repeated over a 30-day period. The survival percentage was calculated by considering the CFUs on day 6 as 100% survival.

Protein methods

The total yeast cell protein precipitation, sample preparation, and western blotting were performed as previously described [52]. Primary antibodies used were rabbit anti-GFP (Abcam, ab290) and rabbit anti-Tubulin (Abcam, EPR13799). The secondary antibody was goat anti-rabbit HRP-conjugated (Advansta #R-05062-500). Chemiluminescence signals were detected using the Bio-Rad Chemidoc MP system. GFP and tubulin band intensities were measured using ImageJ and corrected for membrane background signal. The area sizes measured were kept constant across all time points. Relative GFP levels were calculated by dividing the background-corrected GFP band intensities by the corresponding background-corrected tubulin band intensities.

Spot assay for cell growth comparison on agar plates

Yeast cultures were grown in rich media at 30°C until reaching the stationary phase. The cultures were then adjusted to an OD_{600} of 1, and 10-fold serial dilutions were prepared using sterile 1xPBS. Ten microliters of each serial dilution were spotted onto YPD agar plates and incubated at appropriate temperatures for 1-3 days.

Data presentation and Statistical analysis:

Images were visualized and analyzed using ImageJ, figures assembled in Photoshop, and labeled in Illustrator (Adobe, San Jose, CA, USA). Graphs were plotted using Prism 10.2.3 (GraphPad, Le Jolla, CA, USA), and statistical significance was determined using one-way ANOVA or unpaired two-tailed t-tests as indicated in the figure legends. In Box-and-whisker plots, boxes extend from the 25th to 75th percentiles, whiskers point to the 10th and 90th percentiles, and lines inside the boxes are the median.

Acknowledgements

This study was supported by EMBO installation Grant No. 3918, and TÜBITAK Grant No. 219Z100. MH and MK were funded by TÜBITAK Grant No. 122Z887, 219Z100 and 118Z979 granted to AKC. CD was funded by Koç University. We would like to thank to Gislene Pereira (University of Heidelberg, Germany), Elmar Schiebel (University of Heidelberg, Germany), Andreas Mayer (University of Lausanne, Switzerland), Keisuke Obara (Nagoya University, Japan), Yoshinori Ohsumi (Tokyo Institute of Technology, Japan), Daniel Gottschling (Calico Life Sciences, USA) and Voytek Okreglak (Altos Labs, USA) for sharing yeast strains and plasmids. We are grateful to Jason King (University of Sheffield, UK) for sharing the sequence of the SnxA reporter prior to its release.

Author Contributions

MH, MK and CD designed and performed the experiments. AKC acquired funding, designed experiments, supervised MH, MK and CD. All authors contributed to the writing of the manuscript.

Conflict of Interest

The authors declare that they have no conflict of interest.

Figure legends

Figure 1- SnxA localization at the vacuole periphery is PI(3,5)P_2 dependent.

A-C. Analysis of SnxA-GFP colocalization with the vacuolar marker Vph1-3xmCherry using still images of log-phase cell populations. Representative still images and graphs of PCC values showing SnxA-GFP colocalization with Vph1-3xmCherry are presented. Data shown are comparison of wildtype (WT) cells and PI(3,5)P_2 deficient mutants (MHY286, MHY304, MHY302, and AAY007) in (A), comparison of these cells in A (-) with cells expressing *fab1-ha* (MHY286, MHY288, MHY304, MHY305, MHY302, and MHY303) in (B), and comparison of basal conditions (-) with hyperosmotic shock conditions (+) in (C). Graphs are box-and-whisker plots. Boxes extend from the 25th to 75th percentiles. Lines inside the boxes are the median. Whiskers point to the 10th and 90th percentiles. Ordinary one-way ANOVA

was performed with Fisher's LSD test. ****: $p<0.0001$, ns: non-significant with $p\geq0.2155$. n: sample size. Data shown comes from two independent experiments.

D-E. Analysis of the effect of hyperosmotic shock on SnxA-GFP vacuole periphery localization through time-lapse microscopy. Mean PCC values of SnxA-GFP and Vph1-3xmCherry during the time-lapse series are plotted (D) along with images from selected time points of representative cells (E). The graph represents the mean of PCC values obtained from 20 cells (MHY286) subjected to 0.9 M NaCl treatment. Error bars show the standard error of the mean. Red arrows indicate the time point of NaCl addition to the culture dish.

Scale bars: 3 µm, BF: bright field.

Figure 2- SnxA preferably localizes to the daughter vacuole upon vacuole segregation.

A. Box-and-whisker plots showing PCC values of SnxA-GFP colocalization with the vacuolar marker Vph1-3xmCherry on the mother vacuole (MV) and daughter vacuole (DV) in log-phase WT cells (MHY286) with segregated vacuoles. Boxes show the 25th to 75th percentiles, whiskers point to the 10th and 90th percentiles, and lines inside the boxes are the median. See Figure 1A for representative images. Unpaired two-tailed t-test was performed. ****: $p<0.0001$. Data shown comes from three independent experiments.

B-C. Time-lapse microscopy analysis of the SnxA-GFP localization at the vacuole periphery during the cell cycle of WT cells (MHY286). Image series of selected time points from a representative cell is shown in (B). Time-dependent changes in PCC values of SnxA-GFP colocalization with the vacuolar marker Vph1-3xmCherry on the mother and daughter vacuoles are shown in the graph (C). The graph represents the mean of individual cells aligned with respect to the end of vacuole segregation (t=0). Error bars are the standard error of the mean. The white arrow in B indicates the completion of vacuole segregation (t=0). The periods in which $PI(3,5)P_2$ asymmetry increases (increases), reduces (red.) and disappears are indicated on the graph. Data comes from two independent experiments.

D-E. Analysis of SnxA-GFP localization on the mother and daughter vacuole periphery with respect to the timing of SnxA-GFP signal appearance on the daughter vacuole (DV) relative to the end of vacuole segregation (t=0) (D), and the duration of SnxA-GFP localization on the mother vacuole (MV) and daughter vacuole (DV) periphery (E). Circles on scatter plots indicate measurements of individual cells. Black lines in scatter blots are mean and standard deviation. Data comes from two independent experiments.

F. Time-lapse microscopy-based analysis of SnxA-mCherry localization with respect to spindle elongation in WT cells containing GFP-Tub1 (MHY295). Selected time points from a representative cell are shown. White arrow marks the time point of anaphase onset (t=0) designated by the start of fast spindle elongation. Yellow arrow marks the timing of spindle breakdown as an indicative of mitotic exit. The graph shows the timing of SnxA-mCherry accumulation on the daughter vacuole (arrival at DV) with respect to the anaphase onset (t=0), and SnxA-mCherry disappearance from the daughter vacuole (departure from DV) with respect to the spindle breakdown (t=20).
Scale bars: 3 µm. n: sample size. m: mother, d: daughter

Figure 3- Atg18-mNeongreen localizes predominantly to the daughter vacuole periphery.
A-D. Time-lapse microscopy-based analysis of Atg18-mNeongreen (Atg18-mNG) vacuole periphery localization during the cell cycle in cells containing Vph1-3xmCherry (MUK089). Selected time points from a representative time-lapse series are shown (A) and mean PCC values of Atg18-mNG colocalization with Vph1-3xmCherry are plotted (B). Data is aligned with respect to the timing of vacuole segregation (t=0) in B and the error bars show the standard deviation. White arrow in A indicates the end of vacuole segregation (t=0). Timing of Atg18-mNG appearance on the daughter vacuole with respect to completion of vacuole segregation (C), and persistence of Atg18-mNG signal on both vacuoles (D) are plotted. Ordinary one-way ANOVA was performed with Fisher's LSD test. **** $p<0.0001$. Data comes from 3 independent timelapse experiments.
E. Atg18-mNG daughter vacuole localization with respect to the timing of anaphase onset and spindle breakdown in mCherry-Tub1 containing cells (MUK116). Time-lapse series are of a representative cell are shown. Yellow arrows mark the start of anaphase onset and spindle breakdown respectively. The graph shows Atg18-mNG signal appearance (arrival) and disappearance from the daughter vacuole (departure) relative to the timing of anaphase onset and spindle breakdown, respectively. Data comes from 2 independent timelapse experiments.
Scale bars are 3 µm, n: sample size, DV: daughter vacuole, MV: mother vacuole. Circles in scatter plots are values of individual cells. Black lines in scatter plots represent the mean and standard deviation.

Figure 4- PI3P and Fab1-complex components localize symmetrically on the vacuole periphery.

A. Representative still images and PCC values showing EGFP-2xFYVE colocalization with the vacuolar marker Vph1-3xmCherry in WT cells (MHY252). Unpaired two-tailed t-test was performed. n.s: non-significant with p=0.9036. Data shown is from 2 independent experiments.

B. Representative still images and daughter vacuole to mother vacuole (DV/MV) ratio of Atg18, Atg18-Sloop, Fab1, Vac14 and Vac7 (MUK089, MUK091, SGY008, SGY009, and MUK117) are shown. The red dashed line marks the DV/MV value of 1, which indicates symmetric distribution on both vacuoles without a preference for a specific vacuole. See materials methods for details.

C. Representative still images and PCC values showing SnxA-GFP colocalization with Vph1-3xmCherry on the mother and daughter vacuoles of wildtype (WT) cells and *fab1-ha* or *atg18*Δ mutants (MHY286, MHY288, and MHY289). Data shown is from 2 independent experiments. In the box-and-whisker graphs, boxes show the 25th to 75th percentiles, whiskers show the 10th and 90th percentiles; lines inside the boxes are the mean. In B and C, ordinary one-way ANOVA was performed with Fisher's LSD test. ***: p=0.0002, **** p<0.0001, ns: non-significant with p≥0.7441. Scale bars are 3 µm. BF: bright field.

Figure 5- Asymmetry of PI(3,5)P_2 is critical for asymmetry of vacuolar pH.

A. Assessing relative acidity of mother and daughter vacuoles during the cell cycle of wildtype cells (MHY283). v-SEP-to-mCherry ratios (v-SEP/mCherry) of daughter and mother vacuoles serve as an in vivo pH sensor. The graph shows mean v-SEP/mCherry ratios of five cells. Error bars are standard error of the mean. Cells are aligned with respect to the end of vacuole segregation (t=0). Selected time points from the time series of a representative cell are shown. White arrow marks the time of vacuole segregation (t=0). The periods in which PI(3,5)P_2 asymmetry increases (increases), reduces (red.), and disappears are indicated on the graph based on the Figure 2. Data comes from 2 independent experiments. Scale bars: 3 µm.

B. Representative still images and box-and-whisker plots of v-SEP/mCherry ratios between mother and daughter vacuole in WT (MHY283), *vac7*Δ (MHY291), *fab1-ha* (MHY257), and *vac7*Δ *fab1-ha* (MHY296). Data shown is from 2 independent experiments. Boxes show 25th and 75th percentiles, whiskers indicate 10th and 90th percentiles, the line in the boxes represents the median. Ordinary one-way ANOVA was performed with Fisher's LSD test. **** p<0.0001, ** p=0.0087, ns: non-significant with p≥0.6617. Scale bar:3 µm, BF: bright field.

C. Survival graph of cells with different PI(3,5)P_2 levels and distribution (ESM356, SEY050, SEY084, and SEY213). The data comes from three independent biological replicates, with two technical replicates of each. The graph shows the mean with the standard error of the mean as error bars.

Figure 6- Vacuole acidity depends on Atg18 and its binding to PI3,5P2.

A. Representative still images and v-SEP/mCherry ratios of mother and daughter vacuoles in WT (MHY283) and *atg18*Δ (MHY277) cells. Data shown is from 2 independent experiments.

B. Analysis of vacuolar pH via time-lapse microscopy in *atg18*Δ cells (MHY277). Selected time points from the time series are shown. The graph represents the mean of v-SEP/mCherry ratios of mother and daughter vacuoles as a function of time. Data from individual cells are aligned with respect to the vacuole segregation. Error bars show the standard error of the mean.

C. Analysis of vacuolar pH in log-phase culture of WT (MHY283), *atg18*Δ (MHY277), Atg18-Sloop (MHY315), and Atg18-FGGG (MHY317) cells. Data comes from 2 independent experiments.

D. Analysis of SnxA-mCherry vacuole periphery localization in cells carrying Vph1-GFP and Atg18-GFP Vph1-GBP (MHY285, and MHY297).

E. Effect of constitutive Atg18 targeting to both vacuoles (Atg18-GFP/GBP) on vacuolar pH (MHY283, MHY297, MHY291, and MHY312). Data shown comes from 2 independent experiments.

In box-and-whisker graphs, boxes show the 25th and 75th percentiles, whiskers indicate the 10th and 90th percentiles, and the line in the boxes represents the median. In A, C, E and F, ordinary one-way ANOVA was performed with Fisher's LSD test. **** $p<0.0001$, ** $p\leq0.0093$, *** $p=0.0004$, and ns: non-significant with $p\geq0.6580$. Scale bars: 3 µm. BF: bright field.

Figure 7. Working model. PI(3,5)P_2 accumulates on the vacuoles of the daughter cell while it is depleted from the vacuoles of the mother cell during mid-to-late mitosis. Concomitantly, daughter cell's vacuole becomes acidified, and mother cell's vacuole becomes alkalinized. Thus, presence of PI(3,5)P_2 on the daughter vacuole plays a role in daughter cell's rejuvenation and absence of PI(3,5)P_2 from the mother vacuole leads to mother cell's aging.

Figure S1- SnxA expression does not affect normal cellular function.

A. SnxA-GFP expression levels in different strains. A representative immunoblot was shown in the bottom. Tub1 was used as a loading control. The graph on the top of each band shows the average of anti-GFP to anti-Tub1 band intensity ratios of from 4 experiments. Error bars: standard error of the mean. Strains used: MHY286, MHY288, MHY289, MHY293, MHY304, MHY305, MHY303, MHY302, and AAY007.

B. Box-and-whisker graph and representative images of vacuole diameters in wildtype (WT), vac7Δ and SnxA-GFP containing yeast cells (BBY070, MHY286, and SEY256). Data shown comes from 3 independent experiments. Boxes show 25th and 75th percentiles, whiskers indicate 10th and 90th percentiles, and the line in the boxes represents the median. Ordinary one-way ANOVA was performed with Fisher's LSD test. **** $p<0.0001$, ns: non-significant with $p=0.7079$. Scale bars: 3 µm. BF: bright field.

C. Spot assays that show growth of cells with (+SnxA-GFP) or without SnxA-GFP. Serial dilutions of indicated strains (ESM356-1 and MHY286) were spotted on YPD plates and incubated at indicated temperatures.

Figure S2- SnxA localization in single cells during mitosis

Each row represents an individual cell analyzed through time-lapse microscopy (MHY286). Vph1-3xmCherry served as a vacuole marker. Each square represents a time point. Time point zero on the graph represents the end of vacuole segregation. The presence of SnxA on vacuoles was judged by eye.

Figure S3- Atg18-mNG vacuole localization depends on PI(3,5)P_2.

A. Analysis Atg18-mNG colocalization with Vph1-3xmCherry upon hyperosmotic shock. Atg18, Atg8-Sloop mutant, and Atg18-FGGG mutant C-terminally fused with mNeongreen were analyzed (MUK089, MUK090, and MUK091). Atg18-FGGG mutant served as a negative control for vacuole periphery localization. The PCC value of 0.5, indicated with a red dashed line, was selected as a threshold for vacuole membrane localization based on the PCC data of Atg18-FGGG. Data comes from 2 independent experiments.

B. Atg18-mNG vacuole localization reflects PI(3,5)P_2 levels. PI(3,5)P_2 levels were manipulated through the use of mutants that are deficient in PI(3,5)P_2 (*vac7*Δ and *vac14*Δ), as well as through the use of *fab1-ha* and 0.9M NaCl treatment in combination with wildtype and *vac7*Δ and *vac14*Δ mutants. PCC values of mNG and Vph1-3xmCherry colocalization were

plotted, and representative images were also shown. Analyzed strains: MUK089, MUK098, MUK081, MUK113, MUK080, and MUK110. Data comes from 3 independent experiments. In box-and-whiskers graphs boxes show the 25th and 75th percentiles, whiskers point to the 10th and 90th percentile, and the line in the boxes represents the median.
Ordinary one-way ANOVA was performed with Fisher's LSD test. **** $p<0.0001$, and ns: non-significant with $p=0.9908$. Scale bars are 3 µm.

Figure S4- Atg18 localization in single cells during mitosis.
Each row represents an individual cell analyzed through time-lapse microscopy (MUK089). Vph1-3xmCherry served as a vacuole marker. Each square represents a time point. Time point zero on the graph represents the end of vacuole segregation. The presence of Atg18-NG on vacuoles was judged by eye.

Figure S5. Atg18-GFP vacuolar localization in cells with and without Vph1-GBP. Representative still images and the percentage of cells in which Atg18-GFP localizes on both vacuoles are shown (MHY223, and SEY082). Graph shows mean of three independent experiments. ~100 cells were counted per strain per experiment. Error bars: standard deviation. ****: $p<0.0001$ according to unpaired two-tailed t-test.

Tables and their legends
Table S1. List of strains used in the study
Table S2. List of plasmids used in the study

Description of Supplementary movies
Supplementary movie 1: Timelapse movie of SnxA-GFP Vph1-3xmCherry containing yeast strain (MHY286). The channels from left to right are GFP, mCherry, and merge.
Supplementary movie 2: Timelapse movie of SnxA-mCherry GFP-Tub1 containing yeast strain (MHY295). The channels from left to right are GFP, mCherry, and merge.
Supplementary movie 3: Timelapse movie of vSEP-mCherry containing yeast strain (MHY283). The channels from left to right are GFP, mCherry, and merge.
Supplementary movie 4: Timelapse movie of vSEP-mCherry containing *atg18*Δ yeast strain (MHY277). The channels from left to right are GFP, mCherry, and merge.

References

1. Han BK, Emr SD. Phosphoinositide [PI(3,5)P2] lipid-dependent regulation of the general transcriptional regulator Tup1. *Genes Dev* **25**, 984-995 (2011).

2. McCartney AJ, Zhang Y, Weisman LS. Phosphatidylinositol 3,5-bisphosphate: low abundance, high significance. *BioEssays : news and reviews in molecular, cellular and developmental biology* **36**, 52-64 (2014).

3. Jin N*, et al.* Roles for PI(3,5)P2 in nutrient sensing through TORC1. *Mol Biol Cell* **25**, 1171-1185 (2014).

4. Huda M, Bektas SN, Bekdas B, Caydasi AK. The signalling lipid PI3,5P(2) is essential for timely mitotic exit. *Open Biol* **13**, 230125 (2023).

5. Jin Y, Weisman LS. The vacuole/lysosome is required for cell-cycle progression. *Elife* **4**, (2015).

6. Rutherford AC*, et al.* The mammalian phosphatidylinositol 3-phosphate 5-kinase (PIKfyve) regulates endosome-to-TGN retrograde transport. *J Cell Sci* **119**, 3944-3957 (2006).

7. McCartney AJ*, et al.* Activity-dependent PI(3,5)P2 synthesis controls AMPA receptor trafficking during synaptic depression. *Proc Natl Acad Sci U S A* **111**, E4896-4905 (2014).

8. Gary JD, Wurmser AE, Bonangelino CJ, Weisman LS, Emr SD. Fab1p is essential for PtdIns(3)P 5-kinase activity and the maintenance of vacuolar size and membrane homeostasis. *J Cell Biol* **143**, 65-79 (1998).

9. Sbrissa D, Ikonomov OC, Shisheva A. PIKfyve, a mammalian ortholog of yeast Fab1p lipid kinase, synthesizes 5-phosphoinositides. Effect of insulin. *J Biol Chem* **274**, 21589-21597 (1999).

10. Giridharan SSP*, et al.* Lipid kinases VPS34 and PIKfyve coordinate a phosphoinositide cascade to regulate retriever-mediated recycling on endosomes. *Elife* **11**, (2022).

11. Chen Z*, et al.* TORC1 Determines Fab1 Lipid Kinase Function at Signaling Endosomes and Vacuoles. *Curr Biol* **31**, 297-309 e298 (2021).

12. Barlow-Busch I, Shaw AL, Burke JE. PI4KA and PIKfyve: Essential phosphoinositide signaling enzymes involved in myriad human diseases. *Curr Opin Cell Biol* **83**, 102207 (2023).

13. Duex JE, Nau JJ, Kauffman EJ, Weisman LS. Phosphoinositide 5-phosphatase Fig 4p is required for both acute rise and subsequent fall in stress-induced phosphatidylinositol 3,5-bisphosphate levels. *Eukaryotic cell* **5**, 723-731 (2006).

14. Dove SK, McEwen RK, Mayes A, Hughes DC, Beggs JD, Michell RH. Vac14 controls PtdIns(3,5)P(2) synthesis and Fab1-dependent protein trafficking to the multivesicular body. *Curr Biol* **12**, 885-893 (2002).

15. Lees JA, Li P, Kumar N, Weisman LS, Reinisch KM. Insights into Lysosomal PI(3,5)P(2) Homeostasis from a Structural-Biochemical Analysis of the PIKfyve Lipid Kinase Complex. *Mol Cell* **80**, 736-743 e734 (2020).

16. Duex JE, Tang F, Weisman LS. The Vac14p-Fig4p complex acts independently of Vac7p and couples PI3,5P2 synthesis and turnover. *J Cell Biol* **172**, 693-704 (2006).

17. Bridges D, Ma JT, Park S, Inoki K, Weisman LS, Saltiel AR. Phosphatidylinositol 3,5-bisphosphate plays a role in the activation and subcellular localization of mechanistic target of rapamycin 1. *Mol Biol Cell* **23**, 2955-2962 (2012).

18. Sbrissa D, Shisheva A. Acquisition of unprecedented phosphatidylinositol 3,5-bisphosphate rise in hyperosmotically stressed 3T3-L1 adipocytes, mediated by ArPIKfyve-PIKfyve pathway. *The Journal of biological chemistry* **280**, 7883-7889 (2005).

19. Tsujita K*, et al.* Myotubularin regulates the function of the late endosome through the gram domain-phosphatidylinositol 3,5-bisphosphate interaction. *The Journal of biological chemistry* **279**, 13817-13824 (2004).

20. Jones DR, Gonzalez-Garcia A, Diez E, Martinez AC, Carrera AC, Merida I. The identification of phosphatidylinositol 3,5-bisphosphate in T-lymphocytes and its regulation by interleukin-2. *The Journal of biological chemistry* **274**, 18407-18413 (1999).

21. Dove SK, Cooke FT, Douglas MR, Sayers LG, Parker PJ, Michell RH. Osmotic stress activates phosphatidylinositol-3,5-bisphosphate synthesis. *Nature* **390**, 187-192 (1997).

22. Jin Y*, et al.* Bur1 functions with TORC1 for vacuole-mediated cell cycle progression. *EMBO Rep* **23**, e53477 (2022).

23. Dong XP*, et al.* PI(3,5)P(2) controls membrane trafficking by direct activation of mucolipin Ca(2+) release channels in the endolysosome. *Nat Commun* **1**, 38 (2010).

24. Samie M*, et al.* A TRP channel in the lysosome regulates large particle phagocytosis via focal exocytosis. *Dev Cell* **26**, 511-524 (2013).

25. Hammond GR, Takasuga S, Sasaki T, Balla T. The ML1Nx2 Phosphatidylinositol 3,5-Bisphosphate Probe Shows Poor Selectivity in Cells. *PLoS One* **10**, e0139957 (2015).

26. Dove SK*, et al.* Svp1p defines a family of phosphatidylinositol 3,5-bisphosphate effectors. *EMBO J* **23**, 1922-1933 (2004).

27. Efe JA, Botelho RJ, Emr SD. Atg18 regulates organelle morphology and Fab1 kinase activity independent of its membrane recruitment by phosphatidylinositol 3,5-bisphosphate. *Mol Biol Cell* **18**, 4232-4244 (2007).

28. Gopaldass N, Fauvet B, Lashuel H, Roux A, Mayer A. Membrane scission driven by the PROPPIN Atg18. *EMBO J* **36**, 3274-3291 (2017).

29. Busse RA, Scacioc A, Krick R, Perez-Lara A, Thumm M, Kuhnel K. Characterization of PROPPIN-Phosphoinositide Binding and Role of Loop 6CD in PROPPIN-Membrane Binding. *Biophys J* **108**, 2223-2234 (2015).

30. Vines JH*, et al.* A PI(3,5)P2 reporter reveals PIKfyve activity and dynamics on macropinosomes and phagosomes. *J Cell Biol* **222**, (2023).

31. Stauffer W, Sheng H, Lim HN. EzColocalization: An ImageJ plugin for visualizing and measuring colocalization in cells and organisms. *Sci Rep* **8**, 15764 (2018).

32. Gary JD, Sato TK, Stefan CJ, Bonangelino CJ, Weisman LS, Emr SD. Regulation of Fab1 phosphatidylinositol 3-phosphate 5-kinase pathway by Vac7 protein and Fig4, a polyphosphoinositide phosphatase family member. *Mol Biol Cell* **13**, 1238-1251 (2002).

33. Takatori S, Tatematsu T, Cheng J, Matsumoto J, Akano T, Fujimoto T. Phosphatidylinositol 3,5-Bisphosphate-Rich Membrane Domains in Endosomes and Lysosomes. *Traffic* **17**, 154-167 (2016).

34. Gillooly DJ*, et al.* Localization of phosphatidylinositol 3-phosphate in yeast and mammalian cells. *EMBO J* **19**, 4577-4588 (2000).

35. Obara K, Noda T, Niimi K, Ohsumi Y. Transport of phosphatidylinositol 3-phosphate into the vacuole via autophagic membranes in Saccharomyces cerevisiae. *Genes to cells : devoted to molecular & cellular mechanisms* **13**, 537-547 (2008).

36. Banerjee S, Clapp K, Tarsio M, Kane PM. Interaction of the late endo-lysosomal lipid PI(3,5)P2 with the Vph1 isoform of yeast V-ATPase increases its activity and cellular stress tolerance. *J Biol Chem* **294**, 9161-9171 (2019).

37. Li SC*, et al.* The signaling lipid PI(3,5)P(2) stabilizes V(1)-V(o) sector interactions and activates the V-ATPase. *Mol Biol Cell* **25**, 1251-1262 (2014).

38. Hughes AL, Gottschling DE. An early age increase in vacuolar pH limits mitochondrial function and lifespan in yeast. *Nature* **492**, 261-265 (2012).

39. Henderson KA, Hughes AL, Gottschling DE. Mother-daughter asymmetry of pH underlies aging and rejuvenation in yeast. *Elife* **3**, e03504 (2014).

40. Okreglak V, Ling R, Ingaramo M, Thayer NH, Millett-Sikking A, Gottschling DE. Cell cycle-linked vacuolar pH dynamics regulate amino acid homeostasis and cell growth. *Nat Metab* **5**, 1803-1819 (2023).

41. Caydasi AK, Khmelinskii A, Duenas-Sanchez R, Kurtulmus B, Knop M, Pereira G. Temporal and compartment-specific signals coordinate mitotic exit with spindle position. *Nat Commun* **8**, 14129 (2017).

42. Weisman LS. Yeast vacuole inheritance and dynamics. *Annu Rev Genet* **37**, 435-460 (2003).

43. Harding TM, Hefner-Gravink A, Thumm M, Klionsky DJ. Genetic and phenotypic overlap between autophagy and the cytoplasm to vacuole protein targeting pathway. *J Biol Chem* **271**, 17621-17624 (1996).

44. Yorimitsu T, Klionsky DJ. Atg11 links cargo to the vesicle-forming machinery in the cytoplasm to vacuole targeting pathway. *Mol Biol Cell* **16**, 1593-1605 (2005).

45. Finnigan GC, Cronan GE, Park HJ, Srinivasan S, Quiocho FA, Stevens TH. Sorting of the yeast vacuolar-type, proton-translocating ATPase enzyme complex (V-ATPase): identification of a necessary and sufficient Golgi/endosomal retention signal in Stv1p. *J Biol Chem* **287**, 19487-19500 (2012).

46. Ruckenstuhl C*, et al.* Lifespan extension by methionine restriction requires autophagy-dependent vacuolar acidification. *PLoS Genet* **10**, e1004347 (2014).

47. Sherman F. [1] Getting started with yeast.). Elsevier (1991).

48. Janke C*, et al.* A versatile toolbox for PCR-based tagging of yeast genes: new fluorescent proteins, more markers and promoter substitution cassettes. *Yeast* **21**, 947-962 (2004).

49. Knop M*, et al.* Epitope tagging of yeast genes using a PCR-based strategy: more tags and improved practical routines. *Yeast* **15**, 963-972 (1999).

50. Caydasi AK, Pereira G. Evaluation of the Dynamicity of Mitotic Exit Network and Spindle Position Checkpoint Components on Spindle Pole Bodies by Fluorescence Recovery After Photobleaching (FRAP). *Methods Mol Biol* **1505**, 167-182 (2017).

51. Hu J, Wei M, Mirisola MG, Longo VD. Assessing Chronological Aging in Saccharomyces cerevisiae.). Humana Press (2013).

52. Meitinger F, Palani S, Pereira G. Detection of Phosphorylation Status of Cytokinetic Components.). Springer New York (2016).

Figure 1

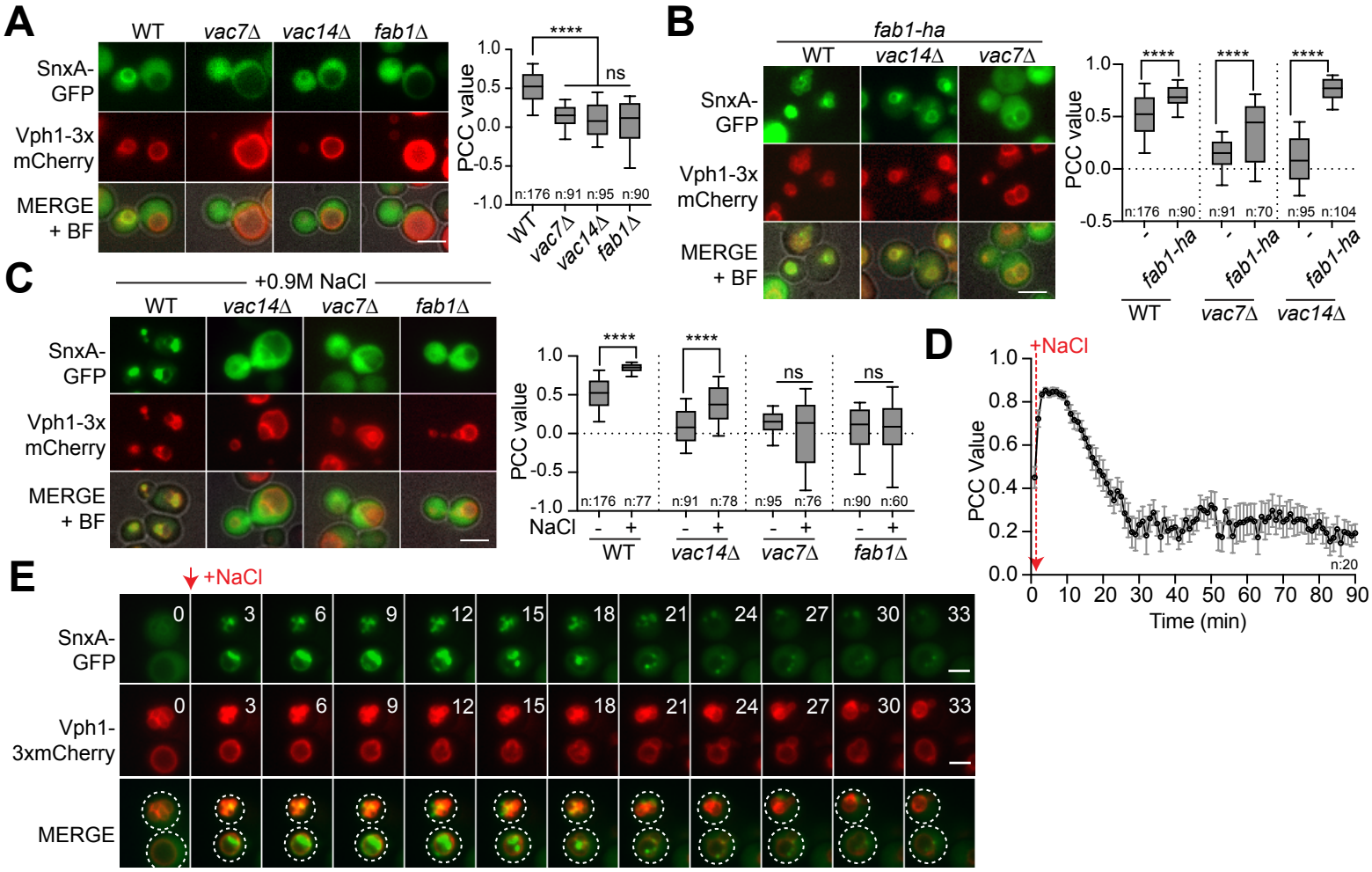
A
WT
vac7Δ
vac14Δ
fab1Δ
SnxA-GFP
Vph1-3x mCherry
MERGE + BF
PCC value
****
ns
n:176 n:91 n:95 n:90
B
fab1-ha
WT
vac14Δ
vac7Δ
n:176 n:90 n:91 n:70 n:95 n:104
C
+0.9M NaCl
n:176 n:77 n:91 n:78 n:95 n:76 n:90 n:60
NaCl
D
+NaCl
PCC Value
Time (min)
n:20
E
+NaCl
0 3 6 9 12 15 18 21 24 27 30 33
Vph1-3xmCherry
MERGE

Figure 2

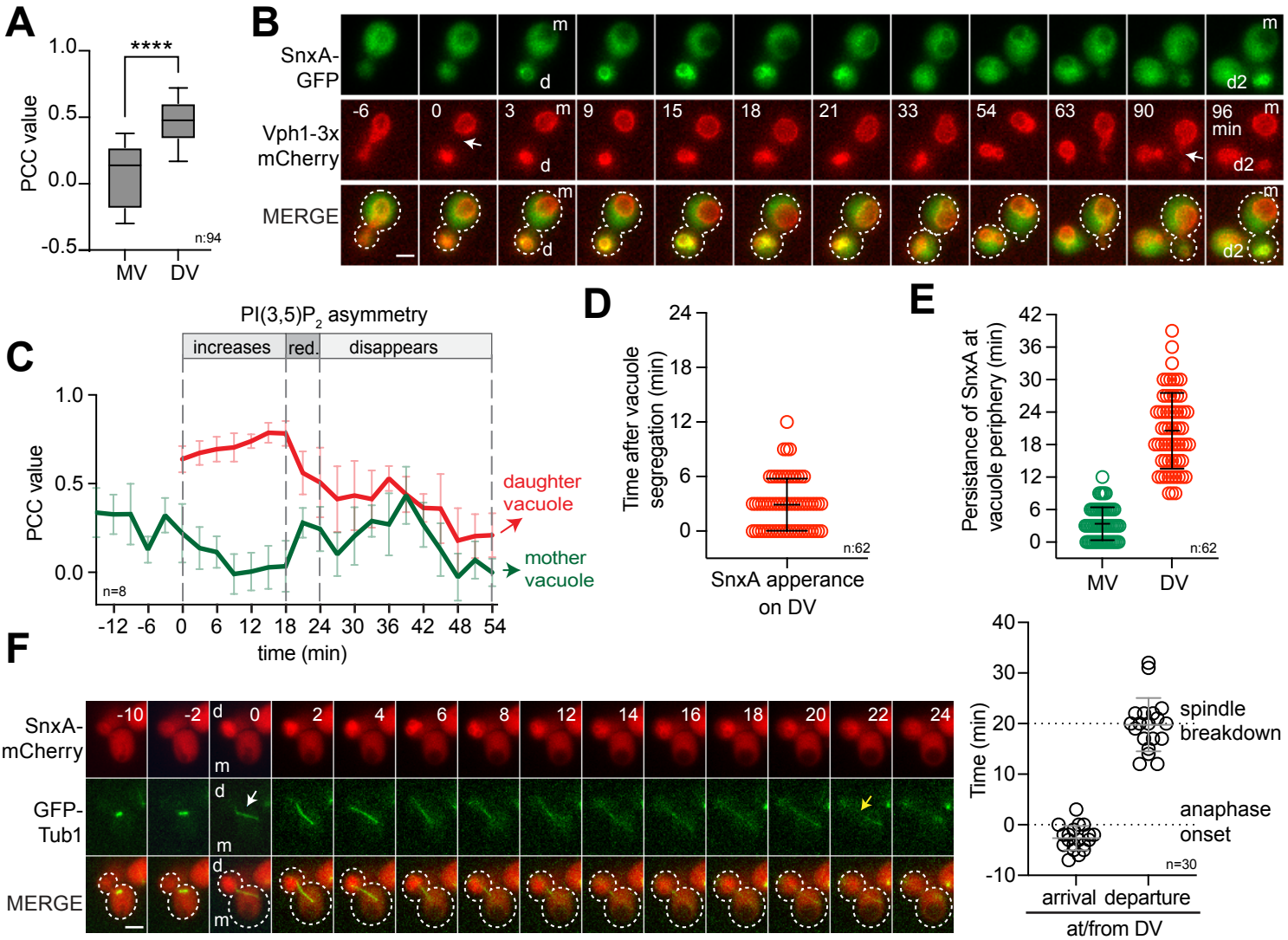
A
PCC value
1.0
0.5
0.0
-0.5
****
n:94
MV
DV
B
SnxA-GFP
Vph1-3x mCherry
MERGE
-6
0
3
9
15
18
21
33
54
63
90
96 min
m
d
d2
C
PI(3,5)P2 asymmetry
increases
red.
disappears
PCC value
daughter vacuole
mother vacuole
n=8
time (min)
D
Time after vacuole segregation (min)
n:62
SnxA apperance on DV
E
Persistance of SnxA at vacuole periphery (min)
n:62
MV
DV
F
SnxA-mCherry
GFP-Tub1
MERGE
-10
-2
0
2
4
6
8
12
14
16
18
20
22
24
Time (min)
spindle breakdown
anaphase onset
n=30
arrival
departure
at/from DV

Figure 3

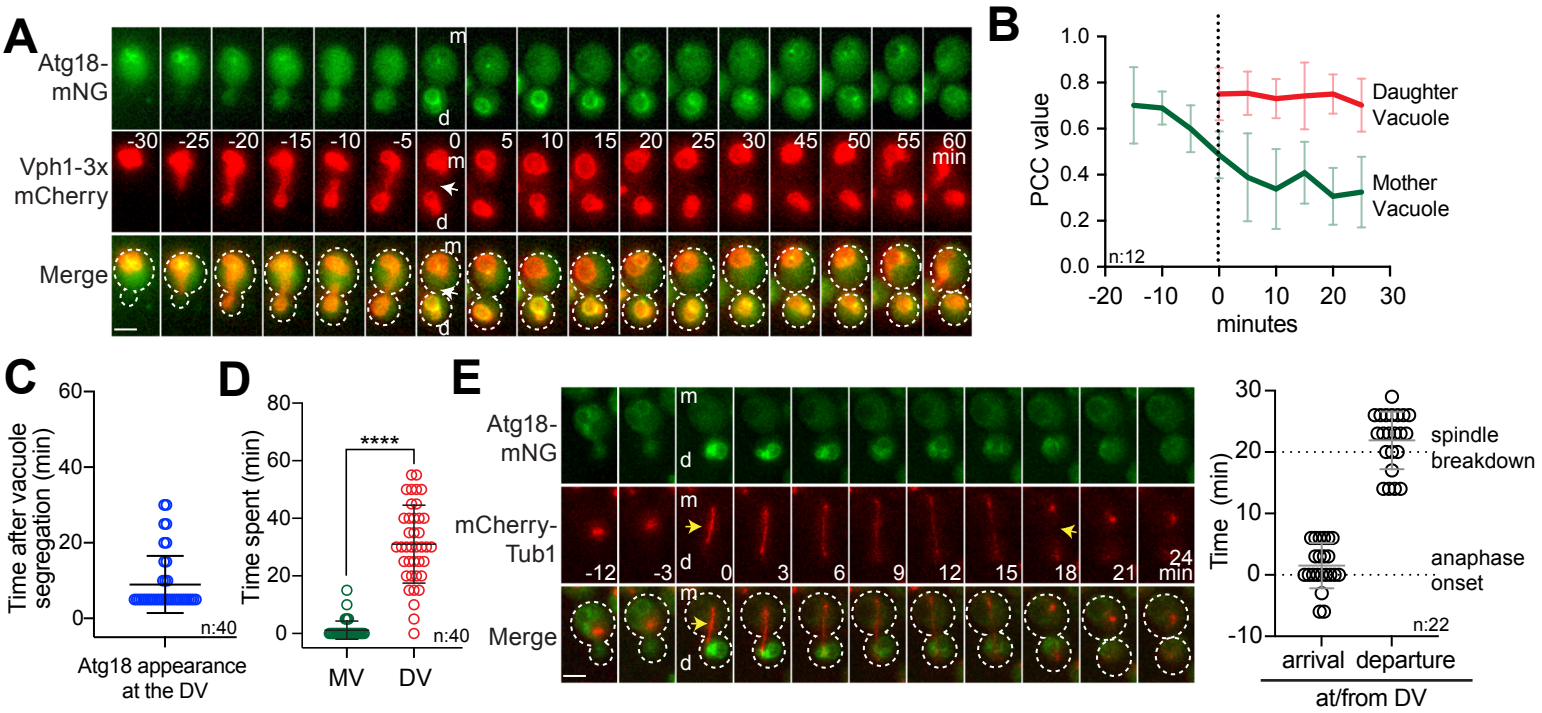
A
Atg18-mNG
Vph1-3x mCherry
Merge
-30 -25 -20 -15 -10 -5 0 5 10 15 20 25 30 45 50 55 60 min
m
d
B
PCC value
minutes
Daughter Vacuole
Mother Vacuole
n:12
C
Time after vacuole segregation (min)
Atg18 appearance at the DV
n:40
D
Time spent (min)
****
MV
DV
n:40
E
Atg18-mNG
mCherry-Tub1
Merge
-12 -3 0 3 6 9 12 15 18 21 24 min
Time (min)
spindle breakdown
anaphase onset
arrival
departure
at/from DV
n:22

Figure 4

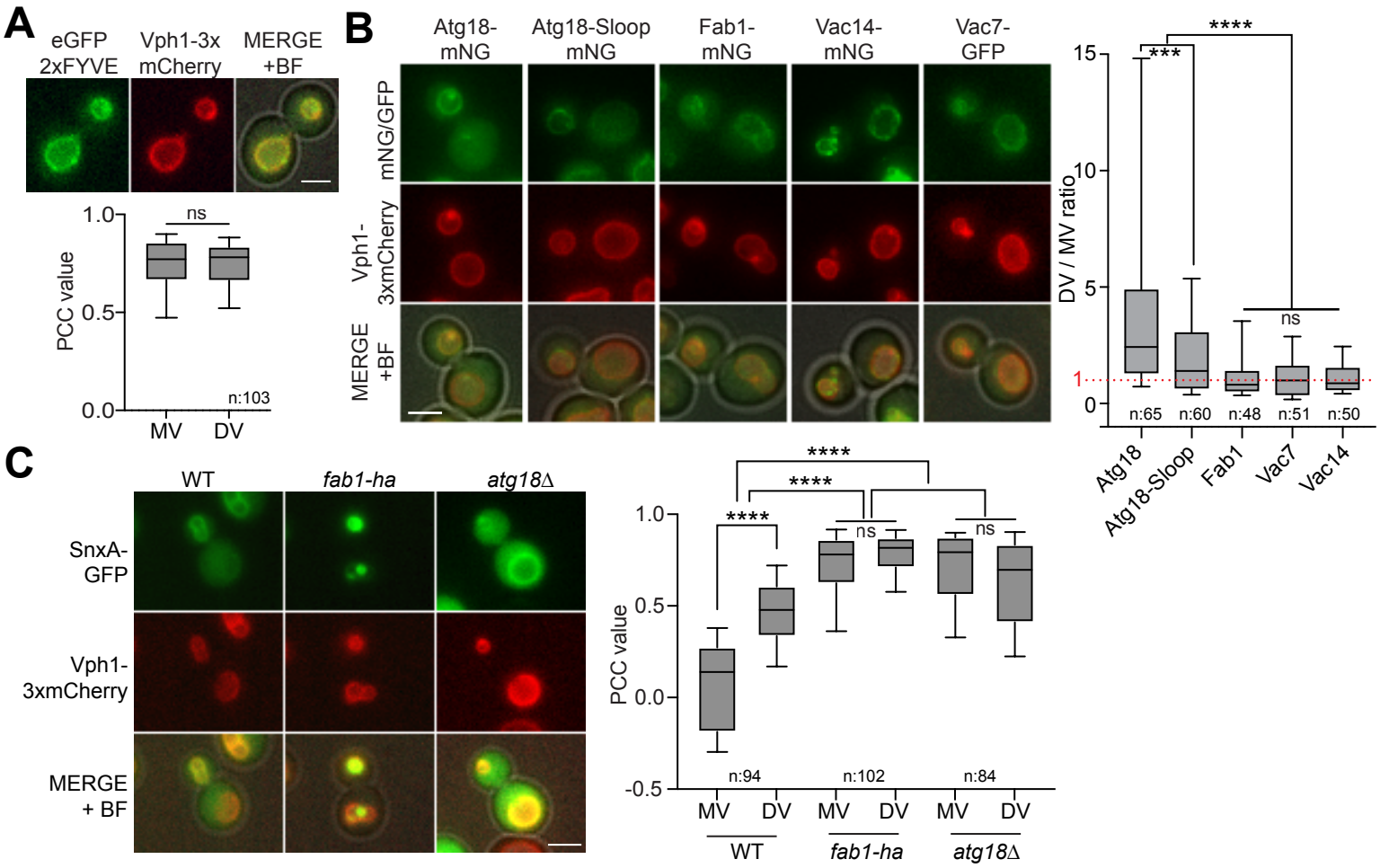
A
eGFP 2xFYVE
Vph1-3x mCherry
MERGE +BF
PCC value
1.0
0.5
0.0
ns
n:103
MV
DV
B
Atg18-mNG
Atg18-Sloop mNG
Fab1-mNG
Vac14-mNG
Vac7-GFP
mNG/GFP
Vph1-3xmCherry
MERGE +BF
DV / MV ratio
15
10
5
1
0
***
****
ns
n:65
n:60
n:48
n:51
n:50
Atg18
Atg18-Sloop
Fab1
Vac7
Vac14
C
WT
fab1-ha
atg18Δ
SnxA-GFP
Vph1-3xmCherry
MERGE + BF
PCC value
1.0
0.5
0.0
-0.5
****
****
****
ns
ns
n:94
n:102
n:84
MV
DV
MV
DV
MV
DV
WT
fab1-ha
atg18Δ

Figure 5

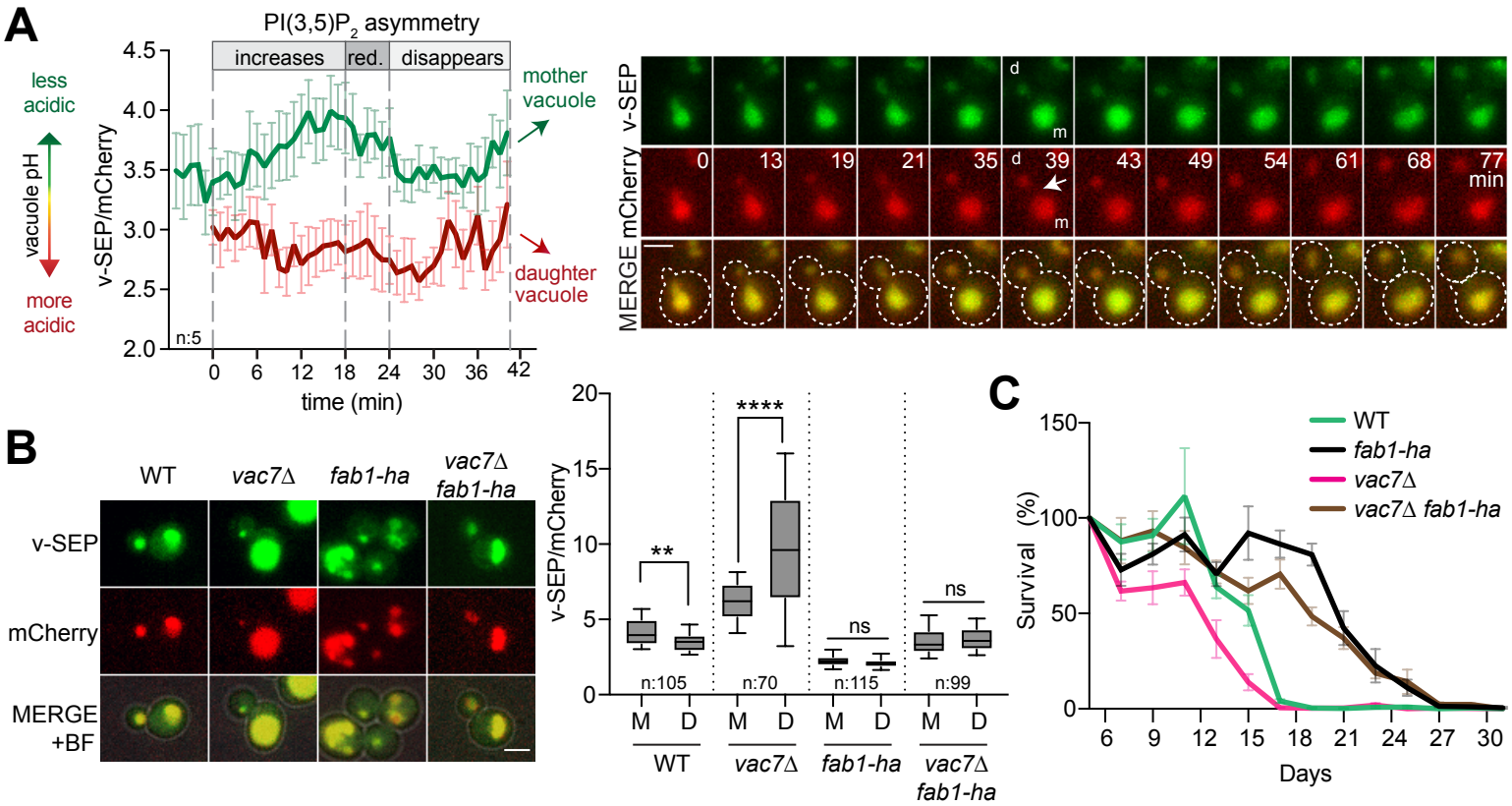
A
PI(3,5)P2 asymmetry
increases
red.
disappears
less acidic
vacuole pH
more acidic
v-SEP/mCherry
mother vacuole
daughter vacuole
n:5
time (min)
v-SEP
mCherry
MERGE
0 13 19 21 35 39 43 49 54 61 68 77 min
d
m
B
WT
vac7Δ
fab1-ha
vac7Δ fab1-ha
v-SEP
mCherry
MERGE +BF
v-SEP/mCherry
**
****
ns
ns
n:105
n:70
n:115
n:99
M D M D M D M D
WT
vac7Δ
fab1-ha
vac7Δ fab1-ha
C
WT
fab1-ha
vac7Δ
vac7Δ fab1-ha
Survival (%)
Days

Figure 6

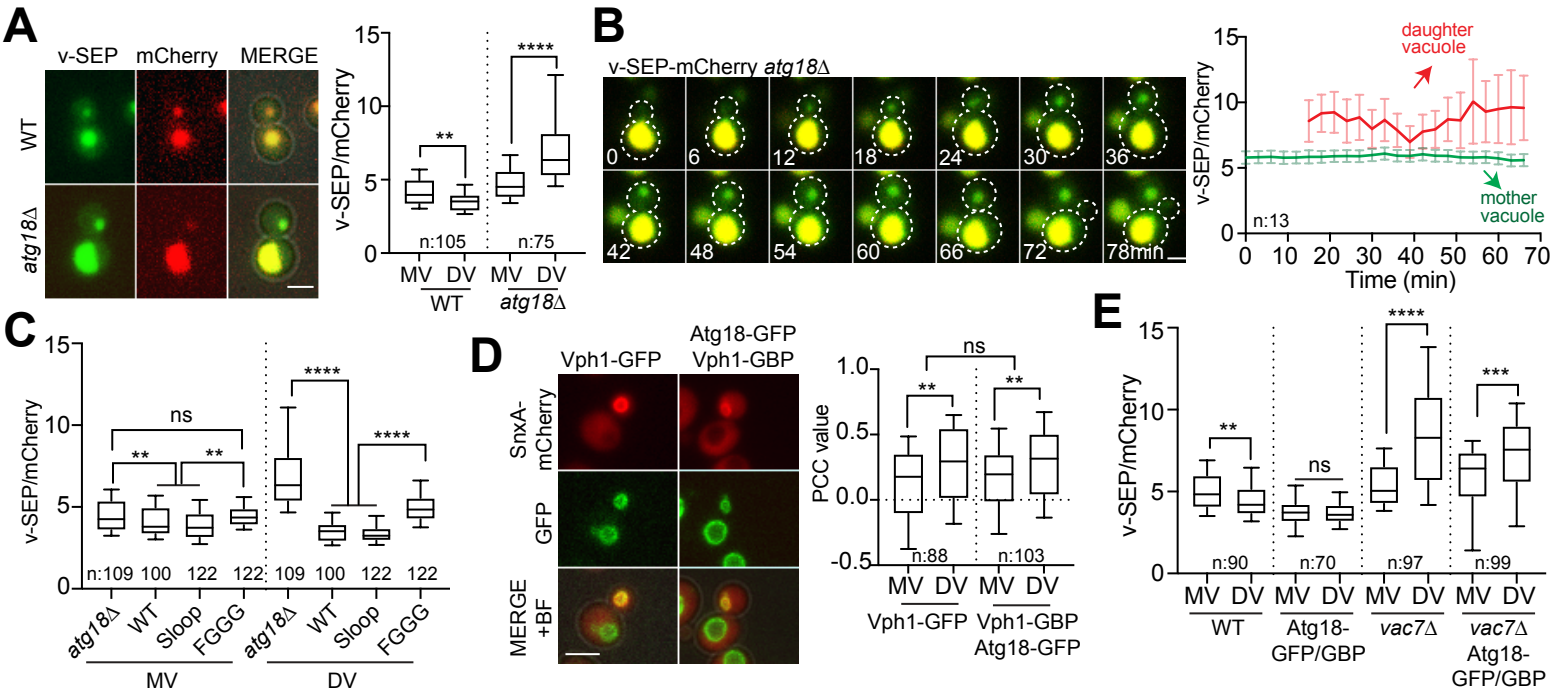
A
v-SEP
mCherry
MERGE
WT
atg18Δ
v-SEP/mCherry
15
10
5
0
**
****
n:105
n:75
MV DV MV DV
WT
atg18Δ
B
v-SEP-mCherry atg18Δ
0
6
12
18
24
30
36
42
48
54
60
66
72
78min
daughter vacuole
mother vacuole
n:13
Time (min)
C
ns
**
**
****
****
n:109 100 122 122 109 100 122 122
atg18Δ
WT
Sloop
FGGG
MV
DV
D
Vph1-GFP
Atg18-GFP
Vph1-GBP
SnxA-mCherry
GFP
MERGE +BF
PCC value
1.0
0.5
0.0
-0.5
n:88
n:103
Vph1-GFP
Vph1-GBP
Atg18-GFP
E
n:90
n:70
n:97
n:99
***
Atg18-GFP/GBP
vac7Δ

Figure 7

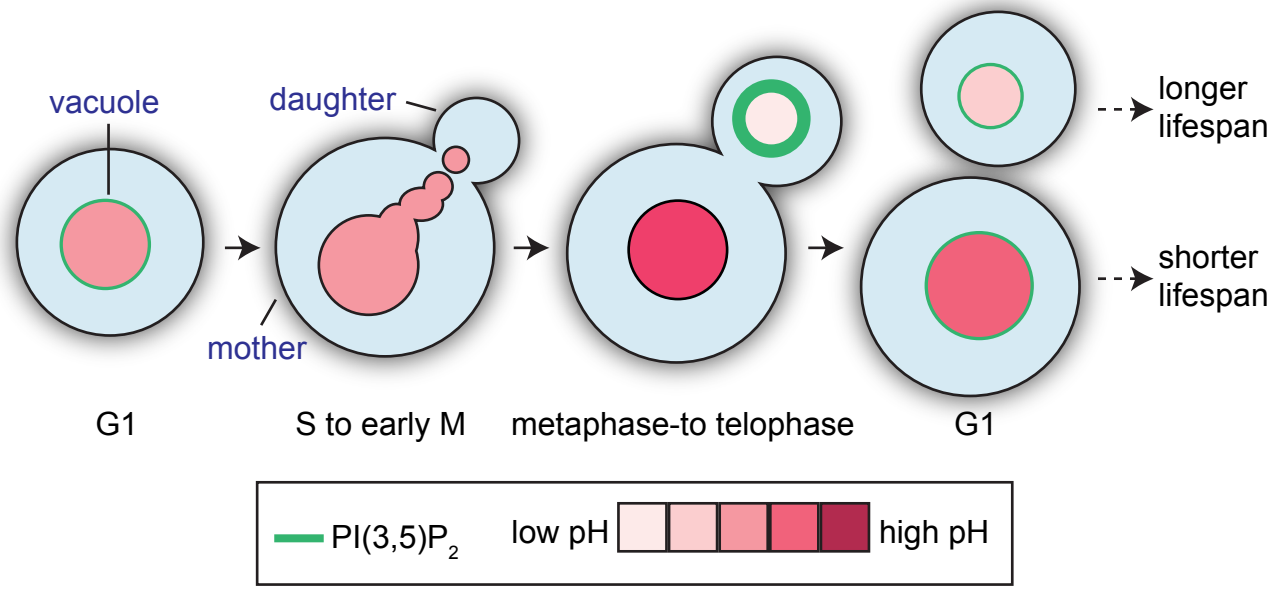
vacuole
daughter
mother
longer lifespan
shorter lifespan
G1
S to early M
metaphase-to telophase
G1
PI(3,5)P2
low pH
high pH